A Neuromorphic Spiking Neural Network Detects Epileptic High Frequency Oscillations in the Scalp EEG

Karla Burelo
UniversitätsSpital und Universität Zürich
Georgia Ramantani
Universitäts-Kinderspital Zürich
Giacomo Indiveri
Institute of Neuroinformatics, University of Zurich and ETH Zurich
Johannes Sarnthein (johannes.sarnthein@usz.ch)
UniversitätsSpital und Universität Zürich

Research Article

Keywords: Interictal High Frequency Oscillations (HFO), Spiking neural networks (SNN)

Posted Date: November 16th, 2021

DOI: https://doi.org/10.21203/rs.3.rs-1061301/v1

Version of Record: A version of this preprint was published at Scientific Reports on February 2nd, 2022. See the published version at https://doi.org/10.1038/s41598-022-05883-8.

Abstract

Background: Interictal High Frequency Oscillations (HFO) are measurable in scalp EEG. This has aroused interest in investigating their potential as biomarkers of epileptogenesis, seizure propensity, disease severity, and treatment response. The demand for therapy monitoring in epilepsy has kindled interest in compact wearable electronic devices for long- term EEG recording. Spiking neural networks (SNN) have been shown to be optimal architectures for being embedded in compact low-power signal processing hardware.

Methods: We analyzed 20 scalp EEG recordings from 11 patients with pediatric focal lesional epilepsy. We designed a custom SNN to detect events of interest (EoI) in the 80-250 Hz ripple band and reject artifacts in the 500-900 Hz band.

Results: We identified the optimal SNN parameters to automatically detect EoI and reject artifacts. The occurrence of HFO thus detected was associated with active epilepsy with 80% accuracy. The HFO rate mirrored the decrease in seizure frequency in 8 patients ($p = 0.0047$). Overall, the HFO rate correlated with seizure frequency (rho = 0.83, $p < 0.0001$, Spearman's correlation).

Conclusions: The fully automated SNN detected clinically relevant HFO in the scalp EEG. This is a further step towards non-invasive epilepsy monitoring with a low-power wearable device.

1. Introduction

1.1 Epilepsy and EEG biomarkers

Epilepsy is one of the most common neurological disorders globally. The standard initial treatment for epilepsy is anti-seizure medication (ASM), resulting in seizure freedom in 60-70% of epilepsy patients, while epilepsy surgery may be an effective treatment option for a subset of the remaining patients with focal lesional epilepsy (1, 2). Monitoring the disease state in epilepsy is the key for assessing the efficacy of ASM or epilepsy surgery in achieving seizure control, and for identifying periods with low or high seizure propensity that will require therapy adjustments over time. Therapy monitoring is crucial for facilitating personalized medicine, thus improving not only seizure outcomes but also quality of life in patients with epilepsy. However, the current gold standard for assessment of any therapeutic intervention in epilepsy is self-reported seizure frequency, i.e. seizure diaries that have often proven unreliable (3-5). In EEG, the presence or absence of epileptiform potentials such as spikes is a sensitive and easily accessible marker of epileptogenicity. However, epileptiform potentials lack a stable correlation with disease activity, undermining their reliability as a biomarker to monitor treatment response (6). Thus, other reliable and practicable biomarkers are urgently needed.

1.2 HFO in the scalp EEG

In recent years, interictal High Frequency Oscillations (HFO), initially recorded directly from epileptogenic brain tissue in intracranial EEG, have been identified as a reliable biomarker of epileptogenicity (7). Only recently, evidence has accumulated that epileptic HFO are also measurable by non-invasive scalp EEG (8-16).

HFO are currently investigated as potential biomarkers of epileptogenesis, seizure propensity, disease severity, and treatment response (for reviews see (7) and (17)). Given the widespread access to non-invasive EEG, scalp HFO may have the potential for clinical assessment in a broad population of patients affected by epilepsy.

1.3 Devices for ultra-long-term epilepsy monitoring

Clinical assessment would greatly benefit from long-term epilepsy monitoring by a wearable device. Wearable devices for out-of-hospital epilepsy monitoring over months or years represent a potential breakthrough in epilepsy diagnosis and treatment, as they may facilitate more accurate seizure detection and thus enable the delivery of therapies with increased efficacy and fewer side effects (18-20). Most current commercial devices aim for seizure detection using non-EEG signals. However, they currently suffer from high false alarm rates; only five current wearable devices perform at a satisfactory level in phase 3 studies (18).

The analysis of scalp EEG signals, among them HFO, may improve epilepsy monitoring. Ultra-long-term recordings of scalp EEG and subcutaneous EEG lasting several months were performed in a research setting (21, 22). They found seizures to occur in cyclical recurrence and showed that around 50% of all seizures remained unnoticed by patients and proxies (comparison of seizure diaries and detected seizures). Compared to current clinical practice, the detection of HFO from scalp EEG recordings may improve epilepsy monitoring. This demands the development of a wearable device that can detect HFO autonomously and for extended periods of time.

1.4 Neuromorphic devices

The large amount of sensory data that is recorded by a wearable device calls for the development of low-power embedded "edge-computing" technologies that can process the signals being measured locally without requiring bulky computers, internet connection, or cloud servers. When developing a wearable sensory-processing device, neuromorphic engineering represents a promising technology.

Neuromorphic electronic circuits are a class of hybrid analog/digital circuits that implement hardware models of biological systems. These circuits can be used to develop a new generation of computing technologies based on the organizing principles of the biological nervous system (23, 24). They carry out computation by emulating the dynamics of real neurons and synapses, configured as small spiking neuronal networks (SNNs). As a consequence, these circuits and networks can be implemented in low-power and compact Very Large Scale Integrated (VLSI) electronic devices to perform real-time computation (23, 25). The styles of computation used in neuromorphic circuits are fundamentally different from those used by conventional computers. Neuromorphic

architectures provide massively parallel arrays of computing elements, exploit redundancy to achieve fault tolerance, and emulate the neural style of computation. In this way, neuromorphic systems can exploit to the fullest potential the features of advanced scaled VLSI processes and future emerging technologies, naturally coping with the problems that characterize them, such as device inhomogeneity and imperfections.

1.5 Hypothesis

In a previous study, we analyzed pediatric scalp EEG and showed that 1) HFO in scalp EEG are associated with HFO in electrocorticography (ECoG), 2) scalp HFO rates correlate with seizure frequency, and 3) scalp HFO rates decrease in response to successful surgical treatment (8). In the current study, we re-analyzed this dataset using a SNN model ideally suited for neuromorphic signal processing hardware. We extended a previously designed SNN that was proven effective in detecting HFO in the presurgical long-term intracranial EEG (iEEG) (26) and in the intraoperative ECoG (27). Here, we tested whether the extended SNN can reliably detect HFO also in the pediatric scalp EEG.

2. Methods

2.1 Patients

We re-analyzed the scalp EEG recordings of children and adolescents with drug-resistant focal lesional epilepsy that underwent presurgical evaluation, resective epilepsy surgery, and postsurgical follow-up (median 45 months) in the University Children's Hospital Zurich and had been considered for our previous study (8). Twenty recordings from 11 patients (8 male) fulfilled the inclusion criteria of scalp EEG 1) recorded at high sampling frequency (>1000 Hz), 2) containing at least 10 min of NREM sleep, and 3) recorded at >2 h from the most recent seizure. In all cases, we could form a clear hypothesis regarding the localization of the epileptogenic zone based on electro-clinical findings and the presence of an MR-visible lesion.

Seizure frequency, as a measure of epilepsy severity, was assessed by long-term video-EEG or seizure diaries at the time of the pre- or postsurgical EEG. Postsurgical seizure outcome was portrayed according to the ILAE scale. Epilepsy substrates were determined by histopathology.

2.2 EEG recordings

All patients underwent routine presurgical and postsurgical EEG using an 8-channel custom-made low-noise amplifier (LNA) with an input noise level of ~2.3 $nV/\sqrt{Hz}$, in addition to the commercial device. Given the limited number of available LNA-channels, we connected four adjacent electrodes over the presumed epileptogenic zone and four homologous electrodes over the contralateral hemisphere. Impedances were typically around 1 kΩ. Data were acquired at 10 kHz and down-sampled to 2 kHz for further processing.

2.3 Data selection

EEG was recorded while patients took afternoon naps. We selected exclusively NREM sleep intervals, since HFO rates are higher during NREM compared to REM sleep (14, 28). Intervals with visible artifacts and channels with continuous interference were excluded from further analysis. The resulting data (mean duration of 27±13 min per patient) was divided into 5-min intervals.

2.4 HFO detection with the Spectrum detector

The Spectrum detector has been described in detail in previous publications (29-33). In brief, the detector has three stages. Stage I determined a baseline amplitude threshold in time intervals with high Stockwell entropy (low oscillatory activity). Events exceeding the threshold were marked as events of interest (EoI). In Stage II, the detector selected all EoI that exhibited a high frequency peak isolated from low frequency activity in the time–frequency space (29). The number of EoI was further reduced in Stage III, where artifacts with multichannel spread were rejected, since HFO are spatially confined in a small patch of cortical tissue (34, 35). Following these steps of automated HFO detection, an observer inspected the events in wideband and filtered in the HFO band to reject further artifacts. This prospective definition of a clinically relevant HFO has been shown to predict postsurgical seizure outcome with high accuracy (30, 32, 33, 36).

2.5 HFO detection with the SNN

The SNN model used is a two-layer network comprising leaky integrate-and-fire (LIF) neurons and synapses with biologically realistic temporal dynamics. To take into account the variability introduced by the neuromorphic analog circuits used to implement the SNN, the hyper-parameters of both synapses and neurons (such as time constant or synaptic weights) were drawn randomly from a normal distribution with coefficient of variation parameters matched to those measured from the electronic circuits (see (26) for details). As a first step in our HFO detection pipeline, we used the EEG front-end signal-processing stages described in our previous work (26, 27). In summary, the wideband EEG (Figure 1a) was filtered in the 80-250 Hz ripple band using 2nd order Butterworth filters (Figure 1b), which are a good approximation of the Tow-Thomas architectures in a hardware implementation of the HFO detector (hardware SNN) (26, 37, 38). We next calculated the background noise in the filtered signal to define a baseline amplitude that had to be exceeded by a putative HFO event (Figure 1c). The threshold for the conversion of the analog signal into spikes was set at 30% of the calculated baseline amplitude. The signal-to-spike conversion algorithm simulated the operations of an asynchronous delta modulator (ADM) circuit (Figure 1d) (26, 39, 40). The ADM produces a positive (UP) spike if the signal increases above a set threshold, from the time it had generated the previous spike. Similarly, it produces a negative (DN) spike, if the signal decreases below the set threshold. The resulting UP-DN spike trains are then provided as inputs to the SNN.

The HFO detection stage of the network consisted of input neurons receiving the UP-DN spikes and a second layer of neurons (Fig. 1e). The projections to the second layer of neurons were via excitatory synapses for UP spikes and inhibitory ones for DN spikes. The synaptic circuits implement biologically plausible dynamics, producing output currents in response to input spikes that decay exponentially. The amplitude of the response and the decay time are set by the synaptic weight parameter and the time constant respectively. For these connections, we used the sets of synaptic time constant and weight parameters that

were previously optimized (26). Additionally, the SNN included a global-inhibitory neuron that constantly suppressed the activity of the neurons in the second layer to avoid their responding to fast transients in the ripple band, and a dis-inhibitory neuron that stopped this inhibition to allow the second layer of neurons to respond to an HFO (27). The parameters for the neurons in the SNN were found heuristically by analyzing HFO and sharp transients in a previous dataset from intraoperative ECoG (27).

In this work, we used this SNN (core SNN) to detect potential HFO. Spikes in the second layer of neurons in the core SNN were used to mark an EoI. Any spike within a 15 ms window indicated an EoI. Consecutive windows containing spikes were concatenated to form a continuous EoI. HFO detection was performed independently for each bipolar channel of the presurgical and postsurgical EEG. There was neither visual inspection nor manual rejection of events in this fully automated algorithm.

We used the Python SNN simulator Brian2 (41), the custom toolbox Teili (42), and the parameters in Table 1 to simulate an SNN that matches the behavior of the neuromorphic circuits of the hardware SNN (26).

Table 1
EEG SNN Parameters.

Connection	Name	Connection strength (fA)	Polarity	Time constant τ (ms)
Input above 500Hz UP spikes to second layer artifact SNN	$S_{up-artifactSNN}$	[7–14]	exc	[3–6]
Input above 500Hz DN spikes to second layer artifact SNN	$S_{dn-\ artifactSNN}$	[7–14]	inh	$S_{up-\ artifactSNN}$ – [0.1-1]
Input ripple UP spikes to second layer core SNN	$S_{up-coreSNN}$	[7–14]	exc	[3–6]
Input ripple DN spikes to second layer core SNN	$S_{dn-\ coreSNN}$	[7–14]	inh	$S_{up-\ coreSNN}$ – [0.1-1]
Input UP spikes to dis-inhibitory neuron	$S_{up-\ di}$	21	exc	5
Input DN spikes to dis-inhibitory neuron	$S_{dn-\ di}$	21	exc	5
Dis-inhibitory neuron to global-inhibitory neuron	S_{di-gi}	17.5	inh	20
Global-inhibitory neuron to second layer core SNN	$S_{gi-\ coreSNN}$	21	inh	5

Synapse parameters of the EEG SNN detector. A connection between two neurons is characterized by the positive (excitatory, exc) or negative (inhibitory, inh) current in fA and the time constant.

The software simulations are compatible with the neuromorphic circuit properties. As the circuits are based on a current-mode design, we used currents to set the network parameters. For example, the time constant for the synapse between the UP input and the dis-inhibitory neuron was set to 21 fA, which corresponds to a time constant of 5 ms (Table 1).

2.6 Clinical validation of HFO

Automated HFO detection, visual validation, and analysis were performed blinded to clinical data. HFO were not used for clinical decision-making.

The output of the HFO detection was compared to whether the epilepsy was active or not in that patient. For each patient, we calculated the HFO rate in each electrode channel of the recordings by dividing the number of HFO detected in the channel by the duration of the recording. We defined a rate threshold of 0.25 HFO/min, as previously computed using the HFO rates found by the Spectrum detector (8). We used the mean HFO rate found in the channels located on the affected hemisphere to relate to whether the epilepsy was active or not. If the HFO rate exceeded the rate threshold, the recording was defined as showing HFO.

We defined as true positive (TP) an EEG showing HFO in patients with active epilepsy (all patients before surgery; patients with postoperative seizure outcome ILAE 2-5). We defined as false positive (FP) an EEG showing HFO in seizure-free patients after surgery (ILAE 1). We defined as false negative (FN) an EEG showing no HFO in patients with active epilepsy. We defined as true negative (TN) an EEG showing no HFO in seizure-free patients after surgery. The positive predictive value (PPV) was calculated as PPV = TP/(TP + FP), the negative predictive value (NPV) as NPV = TN/(TN + FN), the sensitivity = TP/(TP + FN), the specificity = TN/(TN + FP), and the accuracy = (TP + TN)/N, where N indicates the total number of recordings.

2.7 Statistics

The correlation between HFO rate and seizure frequency was estimated using linear regression with ordinary least squares and Spearman's correlation. We compared HFO rates between recordings with the Wilcoxon rank-sum and matched pair signed-rank tests. To test case-wise changes in HFO rate and seizure frequency between presurgical and postsurgical recordings, we used the χ^2 test. Statistical significance was established at $p < 0.05$.

2.8 Ethical considerations

The collection of patient data and the scientific analysis were approved and performed conform to the guidelines and regulations of the ethics committee (Kantonale Ethikkommission Zürich, KEK-ZH PB-2016-02055), and all patients and their parents gave written informed consent.

3. Results

3.1 The SNN for HFO detection in scalp EEG

For our HFO detection pipeline we used the core SNN (Section 2.5), as implemented in our previous studies deriving from iEEG and ECoG recordings (26, 27), and augmented it by an additional SNN for the detection of artifacts in the scalp EEG. We refer to the resulting network architecture as EEG SNN (Figure 1). The goal of the artifact detection SNN is to capture oscillations that may resemble an HFO, but should be rejected based on their high amplitude and frequency.

The core SNN receives input EEG in the 80-250 Hz ripple band. It consists of two input neurons that project the UP and DN spike trains to the second layer of neurons using excitatory and inhibitory synapses, respectively. In addition, the core SNN contains a global inhibitory neuron and a dis-inhibitory neuron that suppress HFO detection during fast transient artifacts in the ripple band. We view the output of the core SNN as EoI.

The artifact detection SNN, specifically designed for this study, processes EEG data simultaneously to the core SNN to suppress HFO detection during fast transient artifacts in the 500-900 Hz band (Figure 1i). The > 500 Hz band was chosen to avoid possible overlap with fast ripple HFO in the 250-500 Hz band.

The artifact detection SNN used the same preprocessing stages as the core SNN but the input signal was filter in the 500-900 Hz frequency band (Figure 1f,g,h). The input EEG was converted to UP and DN spikes that were projected to a second layer of neurons using dynamic synapses. The weights and time constants of the synapses were in the same range as those in the core SNN (Table 1). Any occurrence of a spike in the second layer neurons marked an artifact as the output of the artifact SNN.

We used the spikes that marked an artifact to decide whether an EoI should be classified as an HFO. This step was performed outside of the SNN. The 15 ms time window after a spike was taken as the duration of an artifact. Any EoI overlapping with an artifact was rejected (Figure 2q,h).

3.2 Rejection of HFO in the contralateral channel

Each EEG SNN analyzed the signal of a bipolar EEG channel. To further discard false HFO detections, we eliminated HFO that occurred simultaneously in the homologous channel of the other hemisphere. This elimination was done outside of the EEG SNN. We compared the time points where the EEG SNN detected an HFO in the signals from a channel and its contralateral channel, and eliminated the HFO where the two markings overlapped.

3.3 Example of a detected HFO and a sharp transient artifact > 500 Hz.

Figure 2 shows the activity in the core SNN and in the artifact detection SNN in response to an exemplary HFO and an exemplary artifact.

As an example for an HFO, Figure 2d shows the raster plot of the second layer neurons in the core SNN. Four of these neurons elicited spikes in response to the signal shown in Figure 2a, which indicated the presence of an EoI. Figure 2g shows the raster plot of the second layer neurons in the artifact detection SNN in response to the same signal. None of these neurons responded, meaning that no artifact was detected. Hence, this EoI (Figure 2h: green line) was classified as HFO (Figure 2h: purple line).

As an example for an artifact, Figure 2m shows once again the raster plot of the second layer neurons in the core SNN. In this case, forty-eight of these neurons elicited spikes in response to the signal in Figure 2j, which also indicated the presence of an EoI. However, in this occasion, three of the neurons in the artifact detection SNN elicited a response (Figure 2p) indicating the presence of an artifact in the signal (Figure 2q: yellow line). Hence, this EoI (Figure 2q: green line) was not classified as HFO but as an artifact.

3.4 HFO rates from the SNN and the Spectrum detector are comparable

We next determined the HFO rate. For each patient, we counted the number of HFO detected per electrode channel and divided this number by the duration of the recording (mean 27 min, total data duration 544 min) to obtain the HFO rate (Table 2). We found HFO rates $\geq$ 0.25 HFO/min in the recordings of patients with active epilepsy (100 recording intervals, median duration 4.5 min, median rate 1.4 HFO/min, range [0.11-8.78] HFO/min). The HFO rates of the Spectrum and the SNN detector were correlated (rho = 0.83, $p < 0.0001$ Spearman's rank correlation). In total, the SNN and the Spectrum detector found 6275 HFOs and 5249 HFOs in the affected hemisphere, respectively.

Table 2
Patient characteristics at the pre- and postsurgical EEG recordings.

Patient features			Presurgical EEG recordings			Epilepsy surgery			Postsurgical EEG recordings	
No.	Age, sex	Etiology	Seizure frequency (seizures/month	HFO rate (HFO/min)		Resected area	Follow-up period (months)	ILAE outcome	Seizure frequency (seizures/month	HFO rate (
				Affected Hemisphere	Non-affected Hemisphere					Affected Hemisphe
1	4, f	Sturge Weber syndrome	30	6.38	6.88	R lateral posterior temporal & lateral occipital	51	3	0.2	0.13
2	5, m	FCD 1a	180	5.6	0.54	L medial/lateral anterior temporal	27	5	180	2.05
2	7, m	FCD 1a	180	1.93	1.26	L temporo-posterior, occipital, parietal	67	1	0	0.09
3	10, m	diffuse astrocytoma	0.5	0.66	0.73	R medial anterior temporal	45	3	1	0.79
4	3, m	mMCD	2	0.24	1.1	R medial/lateral anterior temporal	45	5	150	4.1
5	13, m	cavernoma	8	0.88	0.07	L dorsal medial/lateral prefrontal	35	1	0	0.02
6	15, m	DNET	12	0.11	0.22	R medial/lateral anterior temporal	11	1	0	0.03
7	14, f	ganglioglioma	4	0.85	0.15	L inferior/basal temporal	33	1	0	0.05
8	1, f	polymicrogyria, FCD 1a	450	8.78	2.39	R dorsal lateral prefrontal	51	5	4	n/a
9	3, m	FCD 2a	30	n/a	n/a	R dorsal lateral prefrontal	75	1	0	0.1
10	6, f	angiocentric glioma	0.5	n/a	n/a	R dorsal lateral prefrontal	60	5	0.3	0.11
11	17, m	perinatal ischemic lesion	2	n/a	n/a	R lateral posterior temporal & lateral occipital	38	1	0	0.17

Seizure etiology, pre- and postsurgical seizure frequency, lateralization and localization of surgical resection, postsurgical follow-up duration, final seizure out to the ILAE classification, HFO recording channels and rates in the pre- and postsurgical EEG. m: male; f: female; L: left; R: right; FCD: focal cortical dysplasia; malformation of cortical development; DNET: Dysembryoplastic neuroepithelial tumor; ECoG: electrocorticography; HFO: high frequency oscillations.

3.5 Comparison of HFO rates between hemispheres

The SNN found a higher HFO rate in the affected than in the non-affected hemisphere in only 9 of all 14 recordings in patients with active epilepsy. For the remaining five recordings, the HFO rate was lower in the affected than in the non-affected hemisphere. Of these five recordings, three were in patients with deep lesions (Patients 3 & 4). In these two patients, the median HFO rate was 0.57 HFO/min and thus considerably lower than the median HFO rate in the presurgical recordings of patients with more superficial frontal, temporal or occipital lesions (0.97 HFO/min). Over all 14 recordings in patients with active epilepsy, the HFO rates did not differ significantly between the affected and the non-affected hemisphere ($p = 0.3$).

3.6 HFO rates mirror epilepsy severity

Figure 3 illustrates the HFO rate, as recorded before and after surgery, in the exemplary case of Patient 2. This patient underwent resective epilepsy surgery within the left hemisphere and achieved seizure freedom. The decrease of the HFO rate after surgery in this patient mirrored the decrease in seizure frequency

from 180 seizures/month before surgery to seizure freedom after surgery. Table 2 lists the clinical features of our patients and the HFO rates before and after surgery.

HFO rates over the affected hemisphere exceeded the threshold of 0.25 HFO/min in ten EEG recordings, all from patients with active epilepsy (PPV = 100%) and was below this threshold in ten recordings, five of which were from seizure-free patients (NPV = 60%, sensitivity = 71%). The threshold was not exceeded in any of the recordings from seizure-free patients (specificity = 100%). Hence, the SNN associated the HFO rate with active epilepsy with an 80% accuracy (Table 3), which is in line with the prediction of the Spectrum detector in the same dataset (80% accuracy (8)). HFO rates were higher in patients with active epilepsy (20 recordings, $p = 0.003$, Wilcoxon rank-sum test). HFO rate over the affected hemisphere correlated with seizure frequency ($R^2 = 0.66$, $p < 0.00002$, linear regression; $\rho = 0.83$, $p < 0.0001$, Spearman's correlation), as illustrated in Figure 4.

Table 3
HFO association with epilepsy status.

	Spectrum detector prediction [%]	SNN prediction [%]
Specificity = TN/(TN + FP)	67	100
Sensitivity = TP/(TP + FN)	86	71
Negative Predictive Value = TN/(TN + FN)	67	60
Positive Predictive Value = TP/(TP + FP)	86	100
Accuracy=(TP+TN)/N [%]	80	80

Comparison of epilepsy status prediction (active epilepsy: seizures/month > 0) between the Spectrum detector and the SNN. TP True Positive; TN True Negative; FP False Positive; FN False Negative; N = TP + TN + FP + FN = number of patients.

3.7 HFO rates respond to surgical therapy

The decrease in HFO rate over the affected hemisphere corresponded to a decrease in seizure frequency following the full resection of the epileptogenic zone in Patients 5, 6, 7, and Patient 2 (second surgery) (0.88 to 0.02 HFO/min, 0.11 to 0.03 HFO/min, 0.85 to 0.05 HFO/min, and 1.93 to 0.09 HFO/min, respectively), and the partial resection of the epileptogenic zone in Patient 1 (6.38 to 0.13 HFO/min). The increase in HFO rate (0.66 to 0.79 HFO/min and 0.24 to 4.1 HFO/min) reflected an increase in seizure frequency in Patients 3 and 4 (0.5 to 1 seizure/month and 2 to 150 seizures/month). Patient 4 failed to respond to surgery due to an underlying genetic disorder. Postsurgical HFO rate was particularly low (0.02, 0.03, 0.05, 0.1, 0.17, and 0.09 HFO/min) in all patients that achieved seizure freedom (Patient 5, 6, 7, 9, 11, and Patient 2 surgery 2) and particularly high (2.05 and 4.1 HFO/min) in the two patients that remained unaffected by surgery (Patient 2 surgery 1, and Patient 4). Intra-individual decrease in HFO rate between pre- and postsurgical recordings mirrored decrease in seizure frequency (8 cases, $\chi^2_1 = 8$, $p = 0.0047$).

4. Discussion

4.1 Summary of main results

We devised a simulated novel SNN that can automatically detect and correctly distinguish EoI in scalp EEG as artifacts or HFO. The occurrence of HFO was associated with active epilepsy with 80% accuracy. Across all patients and EEG recordings, the HFO rate correlated with seizure frequency. In individual patients, the HFO rate mirrored the decrease or increase in seizure frequency after surgery. We thereby demonstrated the feasibility of HFO detection in scalp EEG with a neuromorphic SNN.

4.2 Comparison with the Spectrum detector

The HFO rates measured by our EEG SNN correlated with the rates detected by the well-stablished and clinically validated Spectrum detector, as applied to the same EEG dataset in our previous work (8). In designing the EEG SNN, we did not aim for one-to-one agreement with the Spectrum detector on the detected HFO events. Rather, we aimed to prove that the HFO rate can be used to determine the epilepsy severity and the seizure frequency of our patients. The two detectors reached agreement on the classification of epilepsy severity and established a significant correlation of HFO rate with seizure frequency.

4.3 Comparison between hemispheres

While the Spectrum detector found a significantly higher HFO rate in the affected than in the non-affected hemisphere ($p = 0.0003$) (8), this was not the case for the SNN ($p = 0.3$). The discrepancy between detectors is most apparent in the HFO rates of the patients with a deep-seated lesion, i.e. where the recording EEG channels were located far from the HFO generator. In these patients, both detectors found smaller HFO rates than in the patients with a more superficial lesion, suggesting a lower signal-to-noise ratio. This observation suggests that the SNN may be more prone to low signal-to-noise ratio than the Spectrum detector.

4.4 SNN features

The core SNN used here has been previously shown to detect clinically relevant HFO in the presurgical long-term iEEG (26) and in the intraoperative ECoG (27), and has been adapted here for HFO detection in the scalp EEG. Our approach for HFO detection using the SNN exploits the simulated temporal dynamics of neurons and synapses to determine the optimal detection parameters compatible with analog circuit distributions. This approach to detect HFO differs considerably from the one followed in deep neural network algorithms, which usually perform very well. However, they are sample-inefficient (i.e., they require

ample computation time) and thus, are unsuitable for implementation in a wearable device. In contrast, the SNN employs a shallow network with carefully tuned weights and time constants, enabling its future implementation in neuromorphic hardware.

4.5 Future implementation in neuromorphic hardware

Our simulated EEG SNN has been motivated by the perspective of a future implementation in neuromorphic processors that carry out computation “at the edge" (43-45). The EEG SNN can be easily mapped onto the neuromorphic device that we have developed and described previously (26). Our neuromorphic device performs pre-processing stages (low-noise amplification, configurable filtering, and signal transformation) and includes a multi-core neuromorphic processor, which supports the implementation of spiking neural networks for solving a wide range of spatio-temporal pattern recognition problems online and in real-time. All parameters and architecture elements in this neuromorphic device have been carefully chosen to enable the implementation of the simulated EEG SNN in the neuromorphic hardware with only minor adaptations. The in-memory computing spike-based processing of our neuromorphic processor results in a compact and battery-powered device that does not interface with other electronic equipment. These characteristics support our aim of long-term EEG recordings for non-invasive epilepsy treatment monitoring.

5. Conclusion

The automated SNN detector ensures a prospective, bias-free definition of clinically relevant HFO in scalp EEG. Scalp HFO rates mirror seizure frequency, and thus epilepsy severity, in pediatric drug-resistant focal epilepsy. Being compatible with neuromorphic technology, the implementation of the EEG SNN in a neuromorphic device might provide a further step towards non-invasive therapy monitoring in patients affected by epilepsy.

Declarations

Data and code availability

The scalp EEG data and the code for the SNN are freely available at our website https://hfozuri.ch/. The scalp EEG data with the HFO markings by the Spectrum detector are freely available at https://gin.g-node.org/USZ_NCH/Scalp_EEG_HFO and the SNN detector can be found at https://github.com/kburel/snn-hfo-detection.

Acknowledgments

We acknowledge grants awarded by the Swiss National Science Foundation (SNSF 320030_176222 to JS and GI). The funders had no role in the design or analysis of the study.

Author Contributions

KB analyzed data, prepared figures and tables. GR treated patients and monitored outcome. JS and GI designed and supervised the study. KB, GR, GI, and JS wrote the article. All authors critically reviewed the manuscript.

Additional Information

Competing interests

The authors declare that they have no competing interests.

References

1. Ryvlin P, Rheims S. Predicting epilepsy surgery outcome. Curr Opin Neurol. 2016;29(2):182–8.
2. Barba C, Cross JH, Braun K, Cossu M, Klotz KA, De Masi S, et al. Trends in pediatric epilepsy surgery in Europe between 2008 and 2015: Country-, center-, and age-specific variation. Epilepsia. 2020;61(2):216–27.
3. Cook MJ, O'Brien TJ, Berkovic SF, Murphy M, Morokoff A, Fabinyi G, et al. Prediction of seizure likelihood with a long-term, implanted seizure advisory system in patients with drug-resistant epilepsy: a first-in-man study. Lancet Neurol. 2013;12(6):563–71.
4. Elger CE, Mormann F. Seizure prediction and documentation–two important problems. Lancet Neurol. 2013;12(6):531–2.
5. Karoly PJ, Eden D, Nurse ES, Cook MJ, Taylor J, Dumanis S, et al. Cycles of self-reported seizure likelihood correspond to yield of diagnostic epilepsy monitoring. Epilepsia. 2021;62(2):416–25.
6. Goncharova, II, Alkawadri R, Gaspard N, Duckrow RB, Spencer DD, Hirsch LJ, et al. The relationship between seizures, interictal spikes and antiepileptic drugs. Clinical neurophysiology: official journal of the International Federation of Clinical Neurophysiology. 2016;127(9):3180–6.
7. Jacobs J, Zijlmans M. HFO to Measure Seizure Propensity and Improve Prognostication in Patients With Epilepsy. Epilepsy Curr. 2020:1535759720957308.

8. Boran E, Sarnthein J, Krayenbuhl N, Ramantani G, Fedele T. High-frequency oscillations in scalp EEG mirror seizure frequency in pediatric focal epilepsy. Scientific Reports. 2019;9(1):16560.
9. Kramer MA, Ostrowski LM, Song DY, Thorn EL, Stoyell SM, Parnes M, et al. Scalp recorded spike ripples predict seizure risk in childhood epilepsy better than spikes. Brain. 2019;142(5):1296–309.
10. Minthe A, Janzarik WG, Lachner-Piza D, Reinacher P, Schulze-Bonhage A, Dümpelmann M, et al. Stable high frequency background EEG activity distinguishes epileptic from healthy brain regions. Brain Communications. 2020;2(2).
11. Nevalainen P, von Ellenrieder N, Klimeš P, Dubeau F, Frauscher B, Gotman J. Association of fast ripples on intracranial EEG and outcomes after epilepsy surgery. Neurology. 2020.
12. Schonberger J, Huber C, Lachner-Piza D, Klotz KA, Dumpelmann M, Schulze-Bonhage A, et al. Interictal Fast Ripples Are Associated With the Seizure-Generating Lesion in Patients With Dual Pathology. Front Neurol. 2020;11:573975.
13. Cai Z, Sohrabpour A, Jiang H, Ye S, Joseph B, Brinkmann BH, et al. Noninvasive high-frequency oscillations riding spikes delineates epileptogenic sources. Proceedings of the National Academy of Sciences. 2021;118(17):e2011130118.
14. Cserpan D, Boran E, Lo Biundo SP, Rosch R, Sarnthein J, Ramantani G. Scalp high-frequency oscillation rates are higher in younger children. Brain Communications. 2021.
15. Klotz KA, Sag Y, Schönberger J, Jacobs J. Scalp Ripples Can Predict Development of Epilepsy After First Unprovoked Seizure in Childhood. Ann Neurol. 2021;89(1):134–42.
16. Tamilia E, Matarrese MAG, Ntolkeras G, Grant PE, Madsen JR, Stufflebeam SM, et al. Noninvasive Mapping of Ripple Onset Predicts Outcome in Epilepsy Surgery. Annals of neurology. 2021;n/a(n/a).
17. Fan Y, Dong L, Liu X, Wang H, Liu Y. Recent advances in the noninvasive detection of high-frequency oscillations in the human brain. Reviews in the Neurosciences. 2020:000010151520200073.
18. Beniczky S, Wiebe S, Jeppesen J, Tatum WO, Brazdil M, Wang Y, et al. Automated seizure detection using wearable devices: A clinical practice guideline of the International League Against Epilepsy and the International Federation of Clinical Neurophysiology. Epilepsia. 2021;62(3):632–46.
19. Cook MJ. Advancing seizure forecasting from cyclical activity data. Lancet Neurol. 2021;20(2):86–7.
20. Proix T, Truccolo W, Leguia MG, Tcheng TK, King-Stephens D, Rao VR, et al. Forecasting seizure risk in adults with focal epilepsy: a development and validation study. Lancet Neurol. 2021;20(2):127–35.
21. Weisdorf S, Duun-Henriksen J, Kjeldsen MJ, Poulsen FR, Gangstad SW, Kjær TW. Ultra-long-term subcutaneous home monitoring of epilepsy—490 days of EEG from nine patients. Epilepsia. 2019;60(11):2204–14.
22. Leguia MG, Andrzejak RG, Rummel C, Fan JM, Mirro EA, Tcheng TK, et al. Seizure Cycles in Focal Epilepsy. JAMA Neurol. 2021.
23. Chicca E, Stefanini F, Bartolozzi C, Indiveri G. Neuromorphic Electronic Circuits for Building Autonomous Cognitive Systems. Proceedings of the Ieee. 2014;102(9):1367-88.
24. Indiveri G, Liu SC. Memory and Information Processing in Neuromorphic Systems. Proceedings of the Ieee. 2015;103(8):1379-97.
25. Rubino A, Livanelioglu C, Qiao N, Payvand M, Indiveri G. Ultra-Low-Power FDSOI Neural Circuits for Extreme-Edge Neuromorphic Intelligence. IEEE Transactions on Circuits and Systems I: Regular Papers. 2021;68(1):45–56.
26. Sharifshazileh M, Burelo K, Sarnthein J, Indiveri G. An electronic neuromorphic system for real-time detection of high frequency oscillations (HFO) in intracranial EEG. Nature communications. 2021;12(1):1–14.
27. Burelo K, Sharifshazileh M, Krayenbühl N, Ramantani G, Indiveri G, Sarnthein J. A spiking neural network (SNN) for detecting high frequency oscillations (HFOs) in the intraoperative ECoG. Scientific Reports. 2021;11(1):6719.
28. von Ellenrieder N, Dubeau F, Gotman J, Frauscher B. Physiological and pathological high-frequency oscillations have distinct sleep-homeostatic properties. Neuroimage Clin. 2017;14:566–73.
29. Burnos S, Hilfiker P, Surucu O, Scholkmann F, Krayenbuhl N, Grunwald T, et al. Human intracranial high frequency oscillations (HFOs) detected by automatic time-frequency analysis. PLoS One. 2014;9(4):e94381.
30. Fedele T, van 't Klooster M, Burnos S, Zweiphenning W, van Klink N, Leijten F, et al. Automatic detection of high frequency oscillations during epilepsy surgery predicts seizure outcome. Clinical Neurophysiol. 2016;127(9):3066–74.
31. Fedele T, Ramantani G, Burnos S, Hilfiker P, Curio G, Grunwald T, et al. Prediction of seizure outcome improved by fast ripples detected in low-noise intraoperative corticogram. Clinical neurophysiology: official journal of the International Federation of Clinical Neurophysiology. 2017;128(7):1220–6.
32. Boran E, Ramantani G, Krayenbuhl N, Schreiber M, Konig K, Fedele T, et al. High-density ECoG improves the detection of high frequency oscillations that predict seizure outcome. Clinical neurophysiology: official journal of the International Federation of Clinical Neurophysiology. 2019;130(10):1882–8.
33. Dimakopoulos V, Mégevand P, Boran E, Momjian S, Seeck M, Vulliémoz S, et al. Blinded study: prospectively defined high-frequency oscillations predict seizure outcome in individual patients. Brain Communications. 2021;3(3).
34. Burnos S, Frauscher B, Zelmann R, Haegelen C, Sarnthein J, Gotman J. The morphology of high frequency oscillations (HFO) does not improve delineating the epileptogenic zone. Clinical neurophysiology: official journal of the International Federation of Clinical Neurophysiology. 2016;127(4):2140–8.
35. Zweiphenning WJEM, van Diessen E, Aarnoutse EJ, Leijten FSS, van Rijen PC, Braun KPJ, et al. The resolution revolution: Comparing spikes and high frequency oscillations in high-density and standard intra-operative electrocorticography of the same patient. Clinical Neurophysiology. 2020;131(5):1040–3.

36. Fedele T, Burnos S, Boran E, Krayenbuhl N, Hilfiker P, Grunwald T, et al. Resection of high frequency oscillations predicts seizure outcome in the individual patient. Sci Rep. 2017;7(1):13836.
37. Fleischer P, Tow J, editors. Design formulas for biquad active filters using three operational amplifiers1973.
38. Sharifshazileh M, Burelo K, Fedele T, Sarnthein J, Indiveri G. A Neuromorphic Device for Detecting High-Frequency Oscillations in Human iEEG. 26th IEEE International Conference on Electronics, Circuits and Systems (ICECS): IEEE; 2019. p. 69-72.
39. Corradi F, Indiveri G. A Neuromorphic Event-Based Neural Recording System for Smart Brain-Machine-Interfaces. IEEE Trans Biomed Circuits Syst. 2015;9(5):699–709.
40. Yang M, Liu S-C, Delbruck TJIJoS-SC. A dynamic vision sensor with 1% temporal contrast sensitivity and in-pixel asynchronous delta modulator for event encoding. 2015;50(9):2149–60.
41. Goodman DF, Brette RJFin. Brian: a simulator for spiking neural networks in python. 2008;2:5.
42. Milde M. Teili: a toolbox for building and testing neural algorithms and computational primitives using spiking neurons. 2018.
43. Pei J, Deng L, Song S, Zhao M, Zhang Y, Wu S, et al. Towards artificial general intelligence with hybrid Tianjic chip architecture. Nature. 2019;572(7767):106–11.
44. Yang S, Deng B, Wang J, Li H, Lu M, Che Y, et al. Scalable Digital Neuromorphic Architecture for Large-Scale Biophysically Meaningful Neural Network With Multi-Compartment Neurons. IEEE Transactions on Neural Networks and Learning Systems. 2020;31(1):148–62.
45. Yang S, Wang J, Hao X, Li H, Wei X, Deng B, et al. BiCoSS: Toward Large-Scale Cognition Brain With Multigranular Neuromorphic Architecture. IEEE Transactions on Neural Networks and Learning Systems. 2021:1–15.

Figures

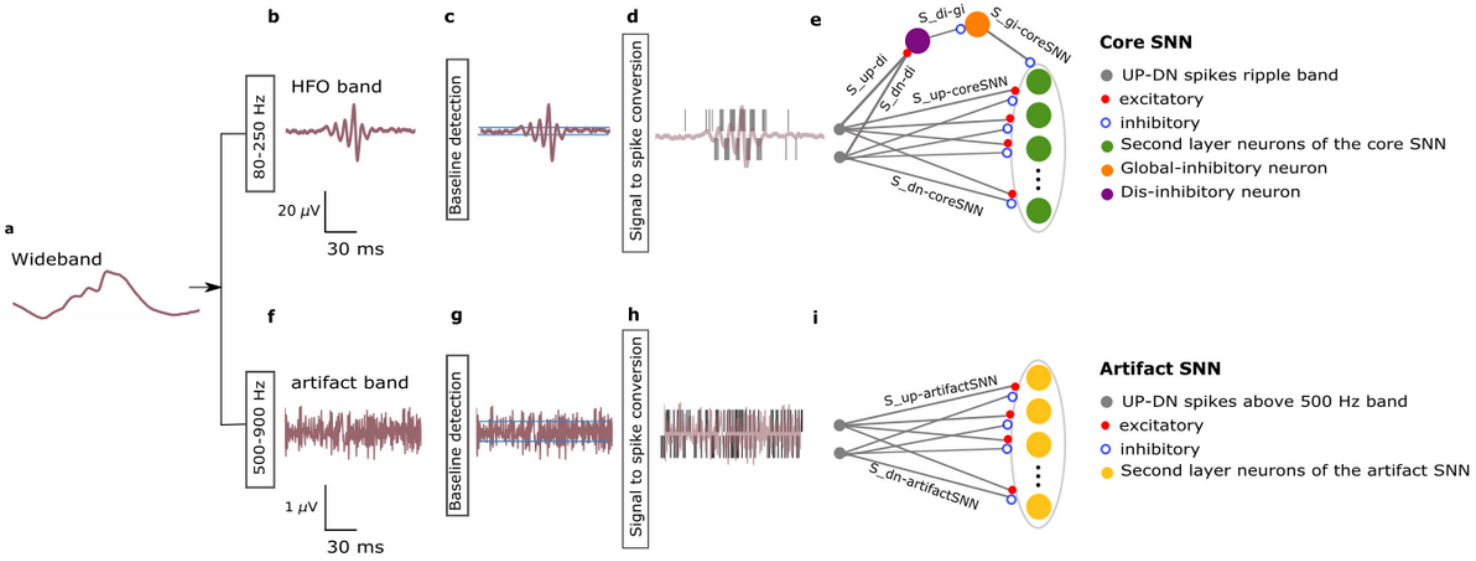

Figure 1

HFO detection scheme The HFO detector performs three preprocessing stages before sending the data to the SNN. The preprocessing stages are filtering, baseline detection, and conversion of the analog signal into spikes. (a) The EEG signal is filtered in the ripple band (80-250 Hz) (b) and above the fast ripple band (500-900 Hz) (f). (c,g) In the baseline detection stage, the background noise of each signal is used to set the signal-to-spike threshold. (d,h) The signal-to-spike conversion algorithm converts each analog signal into two streams of digital outputs: UP and DN spikes. (e) The core SNN architecture for HFO detection consists of input neurons (grey) receiving the input UP-DN spikes from the filtered signal in the ripple band. These inputs project to a second layer of neurons (green) and to a dis-inhibitory neuron (purple). This neuron projects inhibitory synapses to a global-inhibitory neuron (orange), which is continuously inhibiting the second layer neurons. The synapses of the projections are excitatory (positive, red) or inhibitory (negative, blue). The role of the interneuron and the inhibitory neuron is to avoid the false detection of sharp transients (Burelo et al. , 2021).When enough neurons in this layer are activated, they elicit spikes, which indicates the presence of an EoI. (i) The artifact rejection stage of the SNN consists of input neurons (grey) receiving the input UP-DN spikes from the filtered signal above 500 Hz. These inputs project to a second layer of neurons (yellow). When enough neurons in this layer are activated, they elicit spikes, which indicates the presence of an artifact. When the neurons in the core SNN (green) are active at the same time as the neurons in the artifact SNN (yellow), the EoI is rejected. When the neurons in the core SNN (green) are active and the neurons in the artifact SNN (yellow) are silent, the EEG SNN classifies the EoI as HFO.

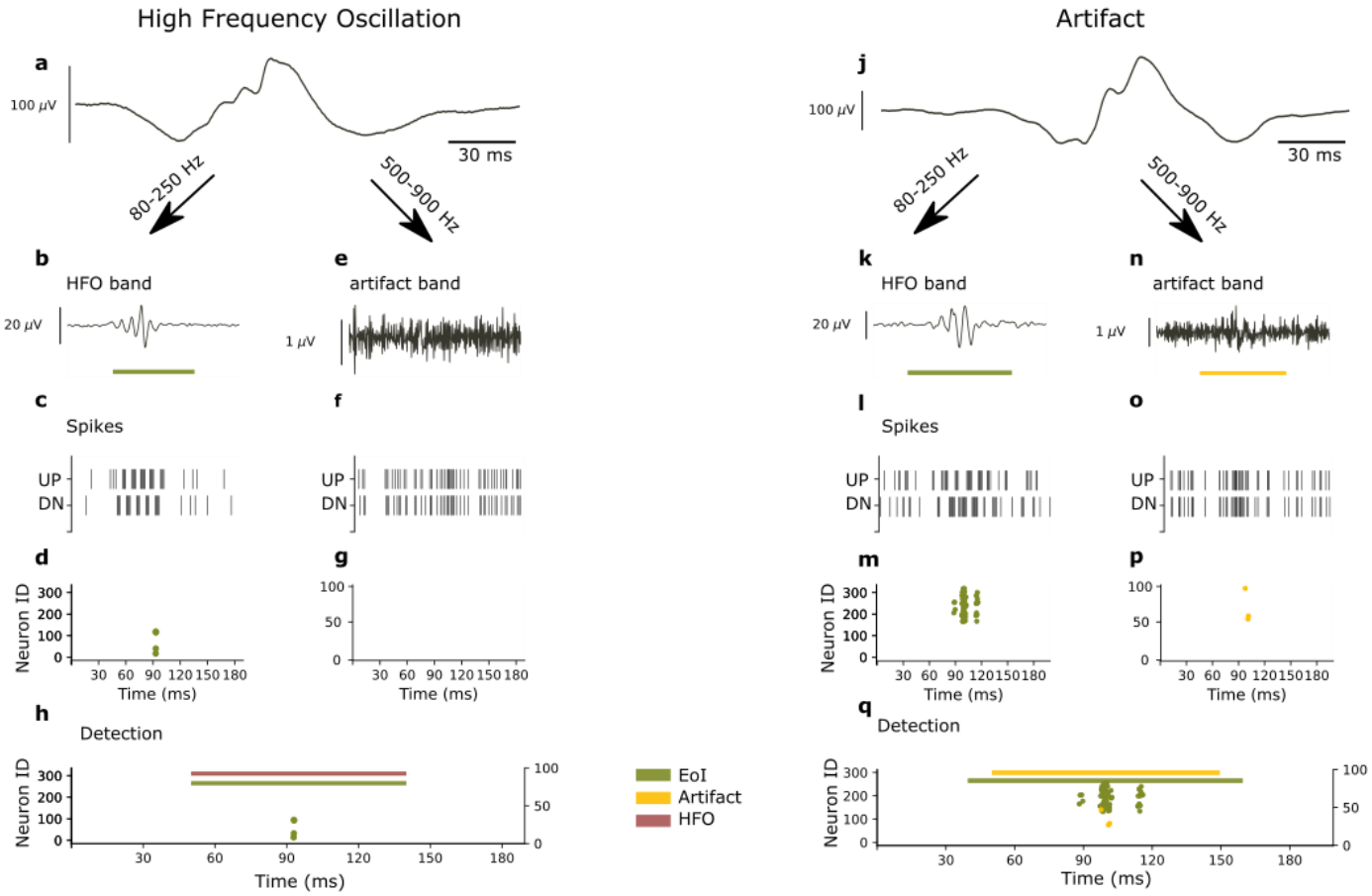

Figure 2

Example of a detected HFO and an artifact The EEG SNN can distinguish if an EoI in the EEG is an HFO or an artifact. (a,j) EEG signal as recorded. (b,k) EEG signal filtered in the ripple band (80-250 Hz). (e,n) EEG signal filtered in the 500-900 Hz band. (c,l) Input spike trains to the core SNN. (g,o) Input spike trains to the artifact detection SNN. (d,m) Raster plot of the neurons in the second layer of the core SNN. (g,p) Raster plot of the neurons in the second layer of the artifact detection SNN. (h, q) Comparison of EoI and artifact marks. For the EEG signal on the left (a), the core SNN indicates an EoI by eliciting spikes (d). The absence of activity from the artifact detection SNN (no spikes in g) indicates that no artifact occurred at this time. (h) The EEG SNN classifies this EoI as HFO. The EEG signal on the right (j) elicits spikes in the core SNN which indicates an EoI (m). The activity from the neurons in the artifact detection SNN (p) indicates that an artifact occurred at this time. (q) The EEG SNN marks this EoI as an artifact.

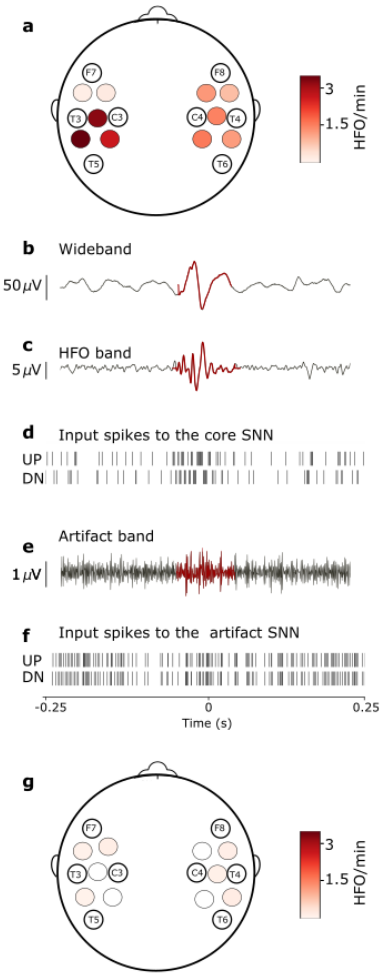

Figure 3

HFO rates in the pre- and post-surgical EEG of Patient 2. HFO rates and their localization in pre- (a) and postsurgical (g) EEG after the second surgery of Patient 2. Example of an HFO detected by the EEG SNN in the presurgical EEG in the bipolar channel T3-T5 (b-f). We filtered the wideband signal (b) in the ripple band (80-250 Hz) (c) and converted it to spikes (d). These spikes are the input to the core SNN for EoI detection. (e) We filtered the same signal in the 500-900 Hz band and converted it to spikes (f). These spikes are the input to the artifact detection SNN for artifact detection. Patient 2 underwent resective epilepsy surgery within the left hemisphere and achieved seizure freedom (follow-up 67 months). The EEG SNN found a 3.5 HFO/min maximum mean HFO rate of in the presurgical and 0.2 HFO/min in the postsurgical recordings. The decrease of HFO rate after surgery in this patient mirrored the decrease in seizure frequency from 180 seizures/month before surgery to postsurgical seizure freedom.

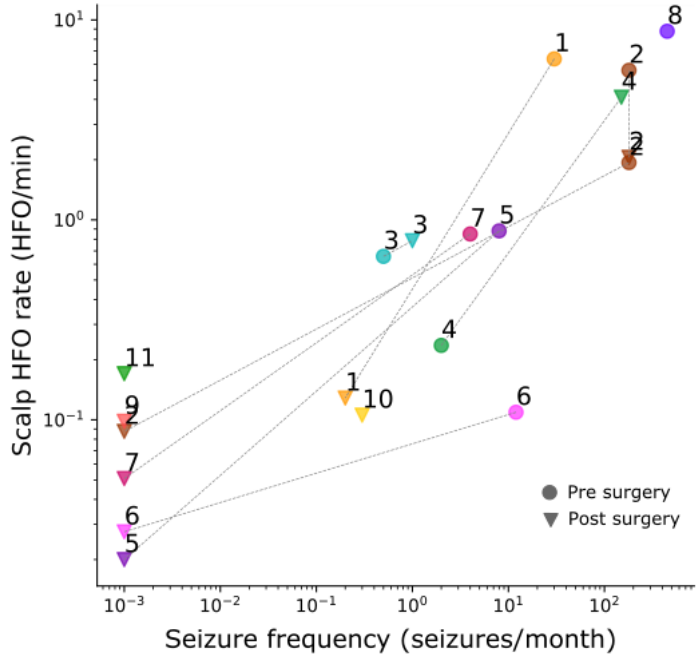

Figure 4

HFO rate mirrors seizure frequency. EEG recordings before (circles) and after (triangles) epilepsy surgery were pooled across our patient cohort. Each point in the plot corresponds to an EEG recording and indicates the seizure frequency and HFO rate at the time of the EEG recording. Axes are in logarithmic scale. For illustrative purposes, seizure freedom was approximated by 0.01 seizures/month. The HFO rate in the EEG correlated with seizure frequency ($R2 = 0.66$, $p < 0.00002$, linear regression; rho = 0.83, $p < 0.0001$, Spearman's correlation).